A Complete Pressure−Temperature Diagram for Air Oxidation of Hydrogen in a Continuous-Flow Stirred Tank Reactor

Robert J. Olsen*

Department of Chemistry, Bard College, Annandale-on-Hudson, New York 12504-5000

Dionisios G. Vlachos

Department of Chemical Engineering, University of Massachusetts, Amherst, Massachusetts 01003-3110

Received: April 6, 1999

We report the temperature and pressure dependence of the dynamics at short residence times of a fuel-lean hydrogen−air mixture in an isothermal continuous-flow stirred tank reactor. The reaction between hydrogen and oxygen is modeled by a set of twenty reversible reactions involving nine species over the temperature and pressure ranges 300−1100 K and 10^{-3}−10 bar, respectively. Boundaries of dynamically distinct regions in a complete pressure−temperature diagram are calculated with a path-following algorithm based on pseudo-arclength continuation. We find a region of birhythmicity, thus showing that chain-branching alone can account for the coexistence of stable oscillatory states, and a region containing a periodic-orbit isola, a new feature for this system. Although infinite-period orbits exist just a few degrees below the ignition curve, oscillatory ignition does not occur under the conditions of our simulations.

Introduction

Combustion is among the oldest fields of science. The unabated need to generate energy while concomitantly reducing pollutant emissions has motivated significant progress in our understanding of combustion chemistry. Still, our knowledge of combustion processes and our ability to control them are often limited by their strongly nonlinear dynamics. Events that are desirable under some circumstances must be avoided at all costs in other situations. For example, while ignition of fuels is an essential step in starting burners, internal combustion engines, and turbines, accidental ignition of a fuel can have catastrophic consequences. Since ignition results from an abrupt change in reaction dynamics, predicting bifurcation features of a reaction model is an integral part of combustion research. Systematic identification of the minimal subsets within a complex reaction network that lead to instabilities can be beneficial both in controlling ignition (by either thermal or kinetic means) and in refining the reaction network. Bifurcation analysis is particularly suited to this task as well. With these factors in mind, we present for the first time a complete two-parameter bifurcation map of a combustion reaction modeled with a detailed kinetic scheme.

The $H_2 + O_2$ Reaction. The gas-phase reaction between hydrogen and oxygen is one of the most thoroughly studied reactions.[1,2] Experiments have been performed in a wide variety of reactors and modeling has been successfully carried out for several reaction sets that differ only in their details. Because it is the simplest system exhibiting chain-branching, the $H_2 + O_2$ reaction is archetypal. That the elementary steps used in modeling the overall reaction are part of all detailed kinetic schemes describing hydrocarbon oxidation further underscores the significance of this reaction. Owing to the wealth of experimental data and well-developed sets of elementary reactions that are available, the $H_2 + O_2$ reaction can serve as a test bed for sophisticated numerical methods; any method that fails when applied to this reaction is unlikely to be useful in the analysis of other combustion reactions.

Experimental observations of oscillatory and steady ignition, coexistence of large- and small-amplitude oscillations (birhythmicity), complex oscillations,[3,4] and chaos[5] have been reported for the $H_2 + O_2$ reaction in a continuous-flow stirred tank reactor (CSTR). Numerical studies of the $H_2 + O_2$ reaction have consistently sought to discern the origins of these dynamical features: are they kinetic or are they are thermokinetic? That is, are they a result of chain-branching alone or of chain-branching and the autocatalytic effect of thermal feedback on reaction rate? Of the reported phenomena, all but oscillatory and steady ignition are thought to be thermokinetically driven.[3,4] Thermokinetic effects are suppressed under isothermal conditions, but strict maintenance of isothermality cannot be experimentally realized for fast reactions such as $H_2 + O_2$, thus making numerical studies an indispensable tool for identifying the source of these dynamical features.

In common parlance ignition is associated with a sudden increase in reaction rate. In a CSTR, this rapid increase in reaction rate is typically linked to loss of stability of a state essentially identical in chemical composition to the mixed but unreacted inlet stream. However, ignition in a CSTR is defined only in part by saying that it is the loss of stability of a state in which there is a negligibly slow rate of conversion of reactants to products. Of equal importance is a description of the state to which the system evolves, and this requires knowing both the types and the stabilities of the states that remain upon disappearance of the extinguished state. In addition to the familiar hysteretic transition between the extinguished state and a steady state of high conversion (*steady ignition*), other examples of ignition are transition to an oscillatory state with a frequency on the order of the residence time and transition without hysteresis to an oscillatory state of large amplitude and very long period (*oscillatory ignition*).[3,4]

* Corresponding author.

10.1021/jp991148b CCC: $18.00
Published on Web 09/16/1999

Sharp bursts of reactivity separated by long intervals during which the extent of reaction is nearly zero characterize oscillatory ignition. Unfortunately, if these characteristics alone are used to define oscillatory ignition, it is then not possible to identify the ignition event with a single type of solution to the rate equations—the characteristics of the final state must be combined with loss of stability of the extinguished steady state. The term oscillatory ignition is not always used in the restricted sense we adopt here. For example, Figure 1 of ref 6 describes an oscillatory state having a period approximately equal to the residence time as oscillatory ignition. More recently, oscillatory ignition was identified with a saddle-node homoclinic bifurcation. This scenario, in which the steady state on the homoclinic orbit undergoes a saddle-node bifurcation, was verified by the absence of hysteresis between the extinguished steady state and the long-period, large-amplitude oscillations and by the way in which the period scaled with the distance from the point at which the steady state lost stability.[4]

Adopting a more restrictive and mathematically formal definition has the advantage of sharpening the goals of a computational study. On the other hand, when considering practical matters such as reactor safety, it may seem like we are making a distinction without a difference. We aim to show that by ascertaining whether oscillatory ignition occurs in the restricted sense, we are able to address the basic mathematical questions with no sacrifice in our ability to discuss practical aspects of reactor dynamics.

Numerical Bifurcation Analysis of the $H_2 + O_2$ Reaction. To analyze the rate equations, we adopt an approach that draws on multiparameter bifurcation theory to explain both local dynamics of steady states and periodic orbits (including the role of distinguished parameters) and global dynamics.[7−9] Viewing the classical pressure−temperature (*p*-*T*) ignition diagram as a two-parameter cross section of the whole of parameter space, we expect to find curves of codimension one bifurcations and isolated points at which codimension two bifurcations occur. The theory of unfolding of degenerate bifurcations is an essential component of numerical bifurcation analysis. Any *p*-*T* diagram we obtain must be vetted by exhaustively comparing one-parameter cross sections to unfoldings described in the dynamical systems literature. Reference 9 is an especially valuable guide to heuristic unfoldings of multiparameter global bifurcations.

Numerical bifurcation analysis has proven itself to be an effective tool in the study of ignition and extinction in both spatially homogeneous and distributed systems.[10] Solutions to the steady-state rate equations are calculated as one of the model parameters is varied. The stability of the solution is immediately assessed via eigenvalue analysis, so accurate detection of bifurcations is an integral feature of the calculations. If bifurcations are detected, additional analyses such as calculation of one-parameter curves of periodic orbits and two-parameter curves of bifurcation points can be undertaken. This should be contrasted with numerical integration of the rate equations using software for initial-value problems. In this case the presence of bifurcations is inferred from inspection of the resulting time series, a potentially error-prone procedure. AUTO86[11] is a robust collection of subroutines that adopts the former, more direct of these two approaches.

In what appears to be the first application of numerical bifurcation analysis of any sort to a detailed kinetic scheme for a combustion reaction, a parent set of 35 reactions for the air oxidation of H_2 was reduced to sets of 10 and 13 reactions and the dynamics in a CSTR of these reduced sets was analyzed using a hybrid approach based on AUTO86 and numerical integration.[12] Curves of steady states were computed by AUTO86. Ignition was found to occur at a transcritical bifurcation; this is puzzling because a transcritical bifurcation is not a generic scenario in one-parameter families of equations. Inspection of the mass balance equations under consideration confirms that they do not possess a trivial solution for which the species' concentrations in the reactor are equal to those in the feedstream. Direct calculation of two-parameter curves of steady-state bifurcations and one-parameter curves of periodic orbits proved elusive, so the portion of the *p*-*T* diagram corresponding to various ignited states was completed via numerical integration. Direct calculation of two-parameter saddle-node and Hopf bifurcation curves and of curves of periodic orbits near Hopf bifurcations using the full set of 35 reactions was reported subsequently.[13]

A hybrid approach (albeit one shifted markedly toward direct methods) has likewise been adopted in a series of recent papers.[14−16] Software written specifically for modeling combustion reactions was used to calculate curves of steady states, detect saddle-node and Hopf bifurcations, calculate two-parameter saddle-node curves, and perform sensitivity and quasi-steady-state analyses along the saddle-node curves. Two-parameter curves of Hopf bifurcations were constructed by extracting the bifurcation points from a series of one-parameter calculations and oscillatory dynamics was investigated by numerical integration. The net result is a fuller account of steady-state behavior and a partial characterization of the oscillatory states. Birhythmicity was detected, but the fate of long-period oscillations remained an open question.[14]

We seek firm numerical evidence for oscillatory ignition and further elucidation of the role of thermal feedback in the $H_2 + O_2$ reaction. Developing a *p*-*T* diagram that is consistent in all respects with local and global two-parameter bifurcation theory is integral to reaching these goals. Since AUTO86 was able to compute complete curves of periodic orbits for liquid-phase reactions in an isothermal CSTR,[17,18] a reexamination of its capabilities for gas-phase reactions is warranted. Following a description of the model we have adopted and further information about the numerical methods we have used, we present several new aspects of the oscillatory dynamics of the $H_2 + O_2$ reaction, discuss ignition and extinction dynamics, and propose experiments that would test the computations.

Model and Methods

For a reaction involving n reactive species in an isothermal CSTR, each species i obeys the mass balance equation[19]

$$\frac{dw_i}{dt} = \frac{R_i M_i}{\rho} - \frac{w_i - w_i^0}{\tau}, \; i = 1, ..., n$$

where w_i is the mass fraction of species i, R_i is the net rate of change of the amount of species i due to chemical reaction per unit volume, M_i is the molar mass of species i, ρ is the mass density calculated assuming the gas mixture behaves ideally, w_i^0 is the mass fraction of species i at the reactor inlet, and τ is the residence time. By choosing isothermal conditions, we are able to identify those aspects of the dynamics that are due to kinetic rather than thermokinetic effects. Since there are one fuel and one oxidant in the feedstream, the inlet mass fractions can be expressed in terms of a single parameter. For this purpose we define the equivalence ratio ϕ as

$$(n_{fuel}/n_{air})_{inlet}/(n_{fuel}/n_{air})_{stoichiometric}$$

TABLE 1: Reactions and Associated Kinetic Parameters[a,b]

	k_o/(mol$^{1-m_i}$ cm$^{3m_i-3}$ s^{-1})	β	E_a/(cal mol^{-1})
R1: $H_2 + O_2 \rightleftarrows 2OH$	1.70×10^{13}	0	4.778×10^4
R2: $H_2 + OH \rightleftarrows H_2O + H$	1.17×10^9	1.30	3.626×10^3
R3: $OH + O \rightleftarrows O_2 + H$	4.00×10^{14}	−0.50	0
R4: $H_2 + O \rightleftarrows OH + H$	5.06×10^4	2.67	6.29×10^3
R5: $O_2 + H + M \rightleftarrows HO_2 + M$[c]	3.61×10^{17}	−0.72	0
R6: $OH + HO_2 \rightleftarrows O_2 + H_2O$	7.50×10^{12}	0	0
R7: $H + HO_2 \rightleftarrows 2OH$	1.40×10^{14}	0	1.073×10^3
R8: $O + HO_2 \rightleftarrows O_2 + OH$	1.40×10^{14}	0	1.073×10^3
R9: $2OH \rightleftarrows H_2O + O$	6.00×10^8	1.30	0
R10: $2H + M \rightleftarrows H_2 + M$[d]	1.00×10^{18}	−1.00	0
R11: $2H + H_2 \rightleftarrows 2H_2$	9.20×10^{16}	−0.60	0
R12: $2H + H_2O \rightleftarrows H_2 + H_2O$	6.00×10^{19}	−1.25	0
R13: $OH + H + M \rightleftarrows H_2O + M$[e]	1.60×10^{22}	−2.00	0
R14: $H + O + M \rightleftarrows OH + M$[f]	6.00×10^{16}	−0.60	0
R15: $2O + M \rightleftarrows O_2 + M$	1.89×10^{13}	0	-1.788×10^3
R16: $H + HO_2 \rightleftarrows H_2 + O_2$	1.25×10^{13}	0	0
R17: $2HO_2 \rightleftarrows O_2 + H_2O_2$	2.00×10^{12}	0	0
R18: $H_2O_2 + M \rightleftarrows 2OH + M$	1.30×10^{17}	0	4.55×10^4
R19: $H + H_2O_2 \rightleftarrows H_2 + HO_2$	1.60×10^{12}	0	3.8×10^3
R20: $OH + H_2O_2 \rightleftarrows H_2O + HO_2$	1.00×10^{13}	0	1.8×10^3

[a] The molecularity and forward rate constant for reaction i are m_i and $k_i = k_{i0}T^{\beta_i}e^{-E_{a,i}/RT}$. [b] Third body efficiencies differing from unity are denoted by $\bar{w}$. [c] $\bar{w}5(H_2) = 2.86$, $\bar{w}5(H_2O) = 18.6$, $\bar{w}5(N_2) = 1.26$. [d] $\bar{w}10(H_2) = 0$, $\bar{w}10(H_2O) = 0$. [e] $\bar{w}13(H_2O) = 5.0$. [f] $\bar{w}14(H_2O) = 5.0$.

Taking the volume fractions of N_2 and O_2 in air to be 0.79 and 0.21, the volume fraction of H_2 in a stoichiometric mixture is 0.296. The four experimentally accessible parameters are τ, ϕ, the reactor temperature T, and the pressure p.

The R_i are calculated using a set of elementary steps comprising twenty reversible reactions of the nine species H_2, O_2, H_2O, H, O, OH, HO_2, H_2O_2, and N_2; the 20 reactions are taken from a comprehensive reaction set for $H_2/O_2/N_2$ combustion chemistry.[20,21] Although N_2 is assumed to be unreactive over the temperature range studied here (300 K < T < 1100 K), it does enter the rate equations as a third-body species. The forward rate constants are given by modified Arrhenius expressions with temperature-dependent preexponentials (see Table 1). Equilibrium constants are computed using the CHEMKIN thermodynamic database[22,23] (beginning from

$$C_{p,i} = a_{0,i} + a_{1,i}T + a_{2,i}T^2 + a_{3,i}T^3 + a_{4,i}T^4$$

conventional enthalpies and entropies of each species i are calculated to account for the temperature dependence of the equilibrium constants). Reverse rate constants are determined by the equilibrium constants and forward rate constants.

Much of the earlier strategy for using AUTO86 to analyze liquid-phase reactions[17,18] was carried over without modification. One important alteration we adopted in this work was tracking the curves of steady states "backwards" from higher to lower extents of reaction. In general, convergence tolerances were less stringent for two-parameter continuations than for one-parameter continuations and for periodic-orbit continuations than for steady-state continuations. Usually all the user-specified tolerances were equal, with typical values being 10^{-10} for one-parameter steady-state continuation, 10^{-6} for two-parameter continuation of steady-state saddle-node or Hopf bifurcations, 10^{-7} for one-parameter periodic-orbit continuation and two-parameter continuation of orbits of fixed period, and 10^{-3} for two-parameter continuation of a periodic-orbit saddle-node bifurcation.

Despite the rather loose tolerances for two-parameter continuation of periodic-orbit saddle-nodes, we found that these curves were in proper registry with individual bifurcation points located to higher precision in corresponding one-parameter continuations of branches of periodic orbits. Computation of an orbit having truly infinite period is not possible using AUTO86. As a consequence, curves of homoclinic orbits were approximated by two-parameter curves of very long period orbits (the period is 2000τ in the figures that follow). Both the tolerances and the stepsize along the branch were decreased when attempting to detect bifurcations of periodic orbits near codimension two points. Tolerances were also decreased in the recalculation of a two-parameter continuation of periodic-orbit saddle-nodes whenever spurious behavior was suspected (insufficiently strict tolerances occasionally caused curves of long-period orbits to coincide with curves of periodic-orbit saddle-nodes). Periodic orbits were typically discretized on a 400 point mesh, with increases in the density of mesh points by up to a factor of 4 in the proximity of degenerate bifurcations. The leading Floquet multiplier often became inaccurate as the branch of periodic orbits became nearly vertical (i.e., as the period approached infinity rapidly); this is a known limitation of the algorithm.[11] In these cases, we relied on direct inspection of the branch as well as dynamical systems theory to reject unnecessarily complicated scenarios. The Jacobian was approximated by finite difference formulas throughout this work.

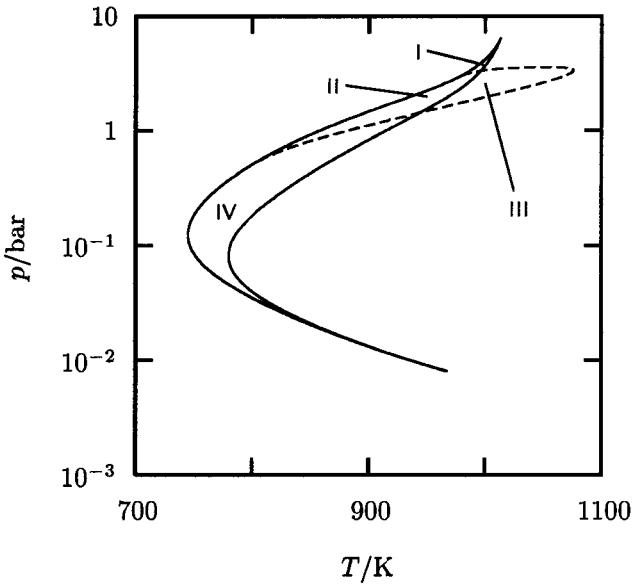

Figure 1. Steady-state bifurcations. Saddle-node (—,SN) and Hopf (- - -,HB) curves are shown as a function of pressure and temperature for $\phi = 0.5$ and $\tau = 1$ ms. Only those regions in which there is not a unique, stable steady state are labeled, and insofar as possible labels are assigned from top to bottom and left to right. A unique steady state coexists with one or more periodic orbits in region III.

New Dynamical Features of the $H_2 + O_2$ Reaction.

We begin by recounting the steady-state bifurcations observed when $\phi = 0.5$ and $\tau = 1$ ms: saddle-node (SN) and Hopf bifurcation (HB) curves are shown in Figure 1. Comparisons to batch reactor dynamics provide a familiar context when interpreting p-T diagrams obtained under flow conditions. For example, the similarity of the right-hand branch of the SN curve to the first and second explosion limits observed in closed vessels is noteworthy and has been discussed previously.[3,14] Unlike in closed systems, the rapid reaction rates following ignition can be sustained in a CSTR due to the continuous influx of reactants. Moreover, as described in the Introduction, other types of ignition may occur.

Inside the crescent-shaped region bounded by the SN curve, three steady states exist, with either one or two of them being

stable. Outside this region, the steady state is unique, and in the unlabeled portion of the *p*-*T* diagram, it is stable. Suppose that pressure is fixed between the lower and upper cusp points and an initial temperature to the left of the crescent is selected. As *T* is increased past the right-hand branch of the SN curve, relatively slow reaction gives way to rapid reaction and the composition of the outflow of the reactor shifts abruptly toward product (here H_2O) from reactants (here H_2 and O_2). For this reason, we designate the initial state and its extension up to the discontinuity as the *extinguished* or *low-conversion* state. In addition to rapid reaction rate and increased product concentrations, states existing past this bifurcation are characterized by significant concentrations of reactive intermediates, and we label such states as *ignited* or *high-conversion*.

In the absence of the HB curve, crossing the right-hand branch of the SN curve in the direction of increasing temperature leads to steady ignition. In the presence of the HB curve, this cannot be true on the segment delimited by the two HB/SN intersections. Crossing the right-hand branch of the SN curve in this pressure range puts the reactor in region III, where the unique steady state is unstable due to the Hopf bifurcation. This implies that ignition to an oscillatory state takes place (the only stable states are oscillatory). Depending on the way in which the stable oscillatory states disappear in this region, ignition to an oscillatory state may occur over an even larger pressure range. To say something more definite about this, we now turn our attention to bifurcations along branches of periodic orbits.

The HB curve begins and ends at Takens−Bogdanov (TB) points on the left-hand branch of the SN curve. Curves of saddle-loop (SL) bifurcations must emanate from these two points.[7] At the TB points, the Hopf and saddle-node bifurcations occur simultaneously. The bifurcations on the left-hand branch of the SN curve have traditionally been associated with extinction. If, as temperature is lowered, the reactor remains in a reactive state until reaching the left-hand branch of the SN curve, a *classical extinction* occurs as this branch is crossed. However, as the Hopf and saddle-node bifurcations separate and the Hopf bifurcation moves to higher temperatures on the ignited branch of steady states, the reactor may extinguish at the Hopf bifurcation rather than at the saddle-node bifurcation. This is an example of *premature extinction*. Premature extinction, first noted in ref 14, is put in a fuller context in the next section. By calculating branches of periodic orbits near the TB points, we learn that close to both endpoints of the HB curve, the Hopf bifurcation is subcritical (i.e., unstable orbits emanate from the bifurcation point), while further from the TB points, the Hopf bifurcation is supercritical. This suggests the presence of at least two degenerate Hopf (H_{10}) points on the HB curve.[7,8] Continuing periodic-orbit branches from the Hopf bifurcation to the saddle-loop bifurcation confirms that near the TB points the infinite-period orbits are unstable, as predicted by the unfolding of the TB point.[7] Similar calculations at some distance from the TB points disclose that the infinite-period orbits are stable at their disappearance. This suggests the presence of at least two trace-zero saddle-loop (TZ) points on the SL curve.[9]

If a curve of periodic-orbit saddle-node (SNP) bifurcations connects an H_{10} point to a TZ point in each instance and the TB points are connected by a single SL curve, a *p*-*T* diagram that is consistent with dynamical systems theory results. This prediction is correct as far as it goes, but filling in the details adds some interesting twists. SNP and SL curves as well as the SN and HB curves near each TB point are shown in Figures 2 and 3. The *p*-*T* diagram has 26 codimension two bifurcation points (see Table 2) and 13 regions with trajectories that are topologically distinct from those in adjacent regions (see Figure 4). Temperature is the distinguished parameter in the reported experimental studies, so we confine the remainder of our discussion by making the same choice.

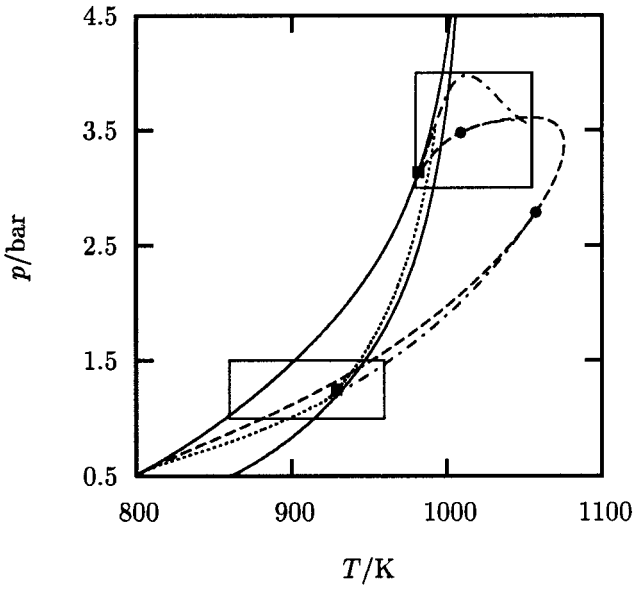

Figure 2. Complete *p*-*T* diagram. Figure 1 is completed by including saddle-loop (···,SL) and periodic-orbit saddle-node (−·−,SNP) curves. Each SNP curve joins a trace-zero saddle-loop point (■,TZ) to a degenerate Hopf point (●,H_{10}). There are no new features at pressures below 0.5 bar. The enclosed areas are redrawn on a larger scale in Figure 3a,b.

The saddle-loop curve has a maximum (quadratic fold) at ^{T}SL; this leads to bifurcation diagrams in which two stable orbits disappear through infinite-period bifurcations. The SNP curve at lower pressure includes a cusp and meets the SL curve at TZ_1. The most striking feature of the complete *p*-*T* diagram is the SNP curve joining the H_{10} and TZ points at higher pressure. This curve possesses two quadratic folds and a cusp. The implications of these three codimension two points are made plain by a series of well-chosen bifurcation diagrams. Taken together, these points give rise to the appearance and disappearance of a periodic-orbit isola (i.e., a branch of periodic orbits not connected to the branch of steady states) and to the existence of intervals of birhythmicity (i.e., intervals in which two stable periodic orbits coexist) for certain values of pressure.

Just as the presence of the HB curve outside the region of steady-state multiplicity guarantees that oscillatory states will be observed in region III of Figure 1, the presence of a segment of the SNP curve outside both the region of steady-state multiplicity and the region enclosed by the HB curve enlarges the area in which oscillatory dynamics is guaranteed. Furthermore, the concurrent presence of the SNP curve and absence of the HB curve near $p(^{T}I^{O})$ signal the existence of isolas of periodic orbits. Figure 5 is a representative bifurcation diagram near this upper pressure limit. As pressure decreases, the isola grows. First, the lower temperature limit of the isola (the left-hand SNP bifurcation) crosses into the interval of steady-state multiplicity, making ignition to an oscillatory state possible. Two Hopf bifurcations and the branch of stable periodic orbits connecting them appear as the pressure decreases past $p(H_{10,1})$. Eventually, the upper temperature limit of the isola (the right-hand SNP bifurcation) exceeds the temperature at the leftmost Hopf bifurcation. Figure 6a shows the resultant birhythmicity. With further decreases in pressure, the amplitude of the periodic orbits continues to grow and the interval of birhythmicity

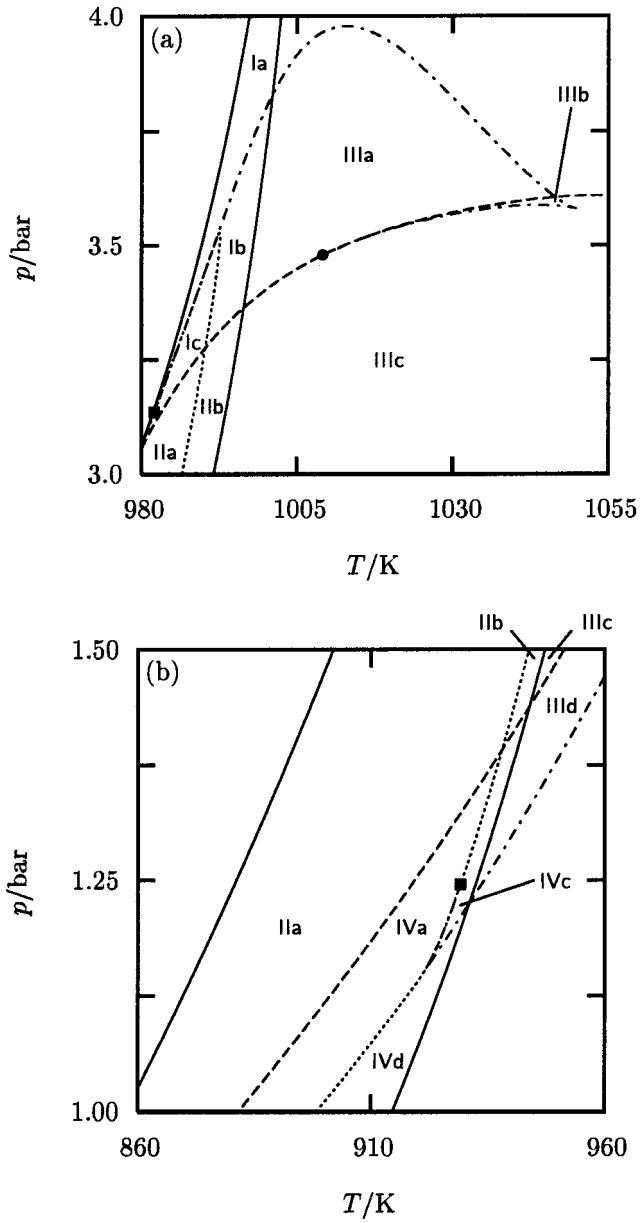

Figure 3. Magnifications of the *p*-*T* diagram. Region III of Figure 1 (now partitioned into subregions IIIb and IIIc) and subregions IIIa and IIId (the areas bounded by the SN, HB, and SNP curves) comprise the new region III. The most notable features of the SNP curve in (a) are the two extrema (quadratic folds) and the cusp. The SNP curve in (b) reverses direction at a cusp that, due to its proximity to the SL curve, is not as prominent as the cusp of (a). Although the SNP and SL curves appear to coincide as they approach the TZ points, there is a sliver of region Ib between the SNP/SL pair near TZ_1 in (a) and the whole of region IVb is between the SNP/SL pair near TZ_2 in (b). Note that region IVb is not visible on the scale shown in (b).

lengthens. At $p({}^{T}\mathrm{S}^{\mathrm{O}})$ the two branches of orbits merge. Between $p({}^{T}\mathrm{S}^{\mathrm{O}})$ and $p(\mathrm{C}_1^0)$ there are four SNP bifurcations and two intervals of birhythmicity on the branch of orbits (see Figure 6b).

Ignition and Extinction: Interpreting the *p*-*T* Diagram.

Having calculated a detailed *p*-*T* diagram, we are able to predict the bifurcation diagram that will be observed for a specified variation of parameter(s). As each bifurcation curve is crossed, the reactor enters a new region of the *p*-*T* diagram; the effect of a bifurcation on the state of the reactor is determined by examining the phase portraits before and after the bifurcation (see Figure 4). Before attempting to explain existing results or anticipate new results in light of Figures 2 and 3, we must adopt several guidelines: (G1) the system behaves as if it were two-dimensional; (G2) a transition between states occurs only if the state in which the reactor existed before a change in parameter does not exist afterward; and (G3) the result of loss of stability of an oscillatory state is determined by the effect of the bifurcation on the basins of attraction of the stable steady states.

TABLE 2: Codimension Two Bifurcations in Order of Decreasing Pressure[a]

bifurcation[b]	symbol[c,d]	(*T*/K, *p*/bar)
steady-state cusp	$\mathrm{C}_1^{\mathrm{S}}$	(1013.3, 6.44)
orbit isola center	${}^{T}\mathrm{I}^{\mathrm{O}}$	(1013.0, 3.98)
SNP_1/SN crossing	$\times_1$	(1001.0, 3.83)
Hopf fold	${}^{T}\mathrm{H}_{01}$	(1053.4, 3.610)
SNP_1/HB crossing	$\times_2$	(1046.5, 3.606)
simple orbit bifurcation	${}^{T}\mathrm{S}^{\mathrm{O}}$	(1043.8, 3.589)
orbit cusp	$\mathrm{C}_1^{\mathrm{O}}$	(1049.45, 3.581)
saddle-loop fold	${}^{T}\mathrm{SL}$	(992.5, 3.528)
saddle-loop fold	${}^{p}\mathrm{SL}$	(992.6, 3.520)
degenerate Hopf bifurcation	$\mathrm{H}_{10,1}$	(1009.2, 3.48)
Hopf fold	${}^{p}\mathrm{H}_{01}$	(1075.6, 3.374)
HB/SN crossing	$\times_3$	(996.37, 3.363)
SL/HB crossing	$\times_4$	(990.20, 3.28)
trace-zero saddle loop	TZ_1	(983.0, 3.17)
Takens-Bogdanov	TB_1	(979.3, 3.03)
degenerate Hopf bifurcation	$\mathrm{H}_{10,2}$	(1055.6, 2.75)
HB/SN crossing	$\times_5$	(943.9, 1.44)
SL/HB crossing	$\times_6$	(938.1, 1.39)
trace-zero saddle loop	TZ_2	(929.2, 1.246)
SNP_2/SN crossing	$\times_7$	(931.1, 1.226)
SNP_2/SL crossing	$\times_8$	(921.5, 1.152)
orbit cusp	$\mathrm{C}_2^{\mathrm{O}}$	(921.3, 1.151)
Takens-Bogdanov	TB_2	(798.0, 0.49)
steady-state isola center	${}^{p}\mathrm{I}^{\mathrm{S}}$	(744.9, 0.13)
simple steady-state bifurcation	${}^{p}\mathrm{S}^{\mathrm{S}}$	(779.6, 0.081)
steady-state cusp	$\mathrm{C}_2^{\mathrm{S}}$	(967.5, 0.0080)

[a] Pressures reported to more than three digits of precision reflect a narrow range of existence for a particular bifurcation diagram due to the presence of another nearby codimension two point. [b] SNP_1 and SNP_2 are the periodic-orbit saddle-node bifurcation curves at high and low pressure. [c] If necessary, a distinguished parameter is identified with a left superscript of *T* or *p*. Right superscripts S and O indicate bifurcations involving steady states and periodic orbits. [d] The designation of two-parameter degenerate Hopf bifurcations by H_{01} and H_{10} follows ref 27. A discussion of the hypotheses of the Hopf bifurcation theorem that are violated at such points can be found in ref 18.

Assumption G1 was used in drawing the phase portraits of Figure 4. One of the implications of G2 is that if the reactor begins in the extinguished steady state, it will remain there until reaching the right-hand branch of the SN curve (see Figure 1). Consideration of the disposition of the stable and unstable directions of the unstable steady state in Figures 4a−c illustrates an application of G3. These directions do not cross on going from 4b to 4a, so it is plausible that the reactor follows a trajectory spiraling into the ignited steady state when the oscillatory state disappears. Conversely, they do cross on going from 4b to 4c, and the ignited steady state is sequestered by the unstable limit cycle, so it seems most reasonable to postulate that the reactor exhibits one or more bursts of reactivity as it spirals away from the unstable limit cycle to the extinguished steady state.

We refer to observations made when the reactor temperature is increased from an initially low value as ignition dynamics. Due to G2, ignition is always associated with the right-hand branch of the SN curve; however, the new state of the reactor varies with pressure. Above $p(\times_1)$ and below $p(\times_8)$, the only remaining stable state is the ignited steady state, so we can assign the pressure intervals from $p(\times_8)$ to $p(\mathrm{C}_2^{\mathrm{S}})$ and from $p(\mathrm{C}_1^{\mathrm{S}})$ to $p(\times_1)$ as steady ignition. Between $p(\times_1)$ and $p(\times_8)$,

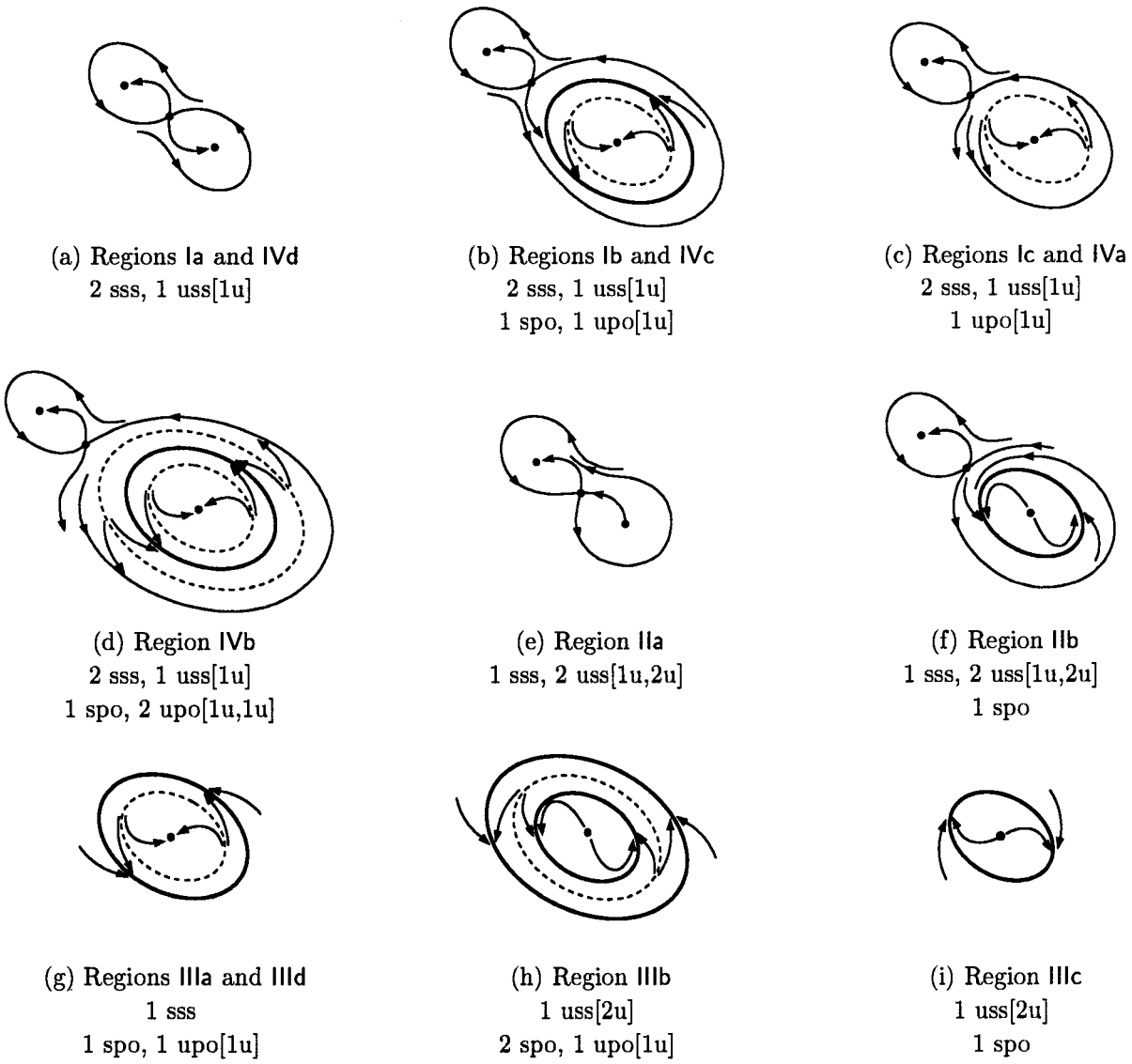

Figure 4. Phase portraits. Stable and unstable steady states are denoted by sss and uss. Stable and unstable periodic orbits are drawn as solid and dashed closed curves and denoted by spo and upo. The unstable states are more properly described as saddles because they have both attracting and repelling character. The number of unstable "directions" associated with these states is given in square brackets. The reactant mole fraction increases in the vertical direction, so in phase portraits with multiple steady states, the ignited steady state is at the lower right.

ignition to an oscillatory state takes place. This follows from G1 because to get to the ignited steady state, the reactor must pass through the stable oscillatory state, which is not possible. Figure 7a shows the relationships between the types of ignition. At lower temperatures, the reactor is extinguished. Oscillatory states are observed in the enclosed area, and steady ignition is observed at higher temperatures. As Figure 7b illustrates, the periodic orbit is not homoclinic to the steady state that disappears upon ignition. This demonstrates that existence of relaxation oscillations is not synonymous with the prevailing definition of oscillatory ignition.

We are likewise able to catalog the extinction dynamics observed when the reactor begins in an ignited steady state and temperature is lowered. Extinction dynamics has received attention primarily as a means of detecting hysteresis. For example, if the point at which the extinguished steady-state loses stability as the temperature is increased differs from that at which the reactor returns to the extinguished state as the temperature is decreased, occurrence of a saddle-node homoclinic bifurcation can be ruled out. Ultimately, the reactor must return to the extinguished steady state, but this return can take place either from an oscillatory state or from the continuation of the initial ignited steady state. Oscillatory states can appear and disappear on the ignited branch and can undergo discontinuous changes in amplitude.

By analogy with the classical explosion limits, we define the first and second *extinction limits* as the segments of the left-hand branch of the SN curve below and above the fold. Along the entire first extinction limit and up to $p(TB_2)$, the only possible transition is from an ignited to an extinguished steady state, so we restrict our attention to pressures greater than $p(TB_2)$. Figure 8a,b summarizes extinction dynamics found at pressures between 1 and 4 bar. As pressure increases beyond $p(TB_2)$, a Hopf bifurcation destabilizes the ignited steady state before the left-hand branch of the SN curve is reached. Because the only stable state between TB_2 and C_2^O is the extinguished steady state, premature extinction takes place at the Hopf bifurcation. Stable oscillatory states do exist above $p(C_2^O)$, but extinction of the ignited steady state continues to occur along the HB curve until the reactor passes through regions IVc and IIb in succession (see Figures 3b, 4b, and 4f). This happens when the Hopf point is found at higher temperatures than the saddle-loop point (i.e., at pressures above $p(\times_6)$). Then loss of stability of the ignited steady state causes the reactor to evolve

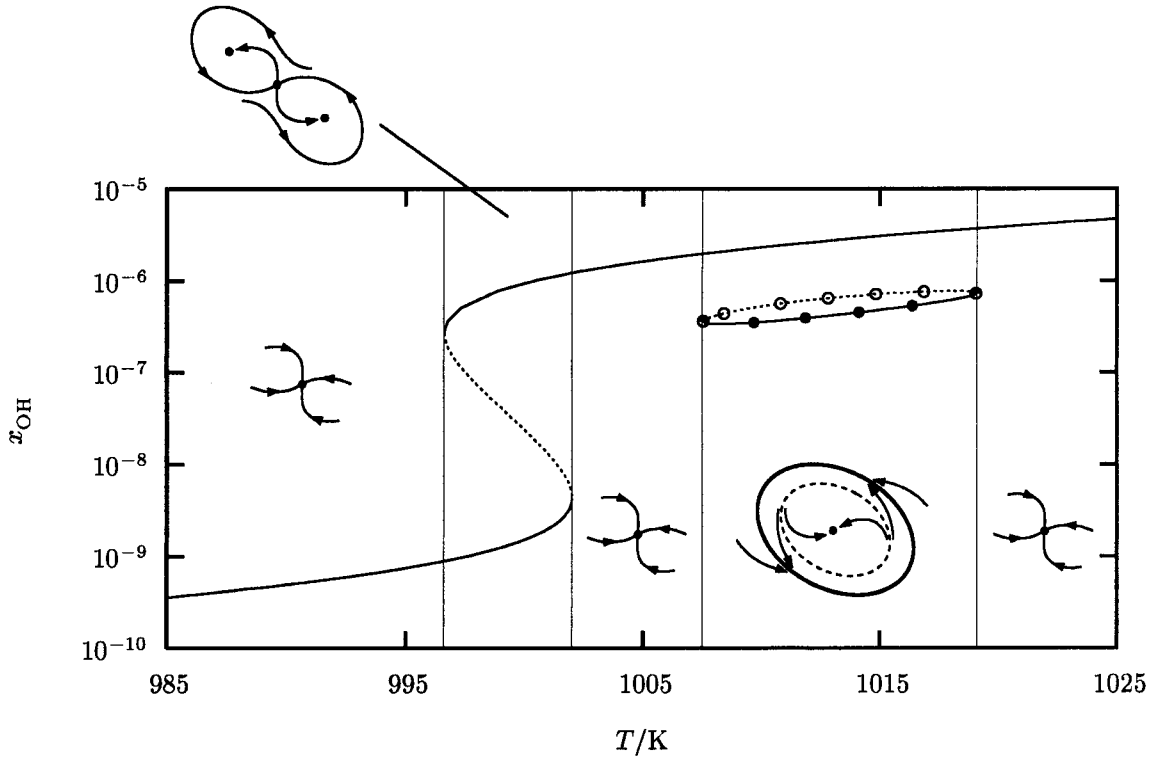

Figure 5. Annotated bifurcation diagram at $p = 3.90$ atm (3.95 bar). Branches of stable and unstable steady states are denoted by — and ···; branches of stable and unstable periodic orbits are denoted by ●● and ··⊙··; and periodic-orbit saddle-node points are denoted by ···◓—. Mole fraction rather than mass fraction is plotted on the ordinate to facilitate interpretation of the bifurcation diagram. Calculations are performed with pressure in atmospheres to maintain backward compatibility among software modules; the corresponding pressure in bar is provided to facilitate comparison with Figures 1−3 and Table 2.

to an oscillatory state having large amplitude; extinction from this oscillatory state occurs when the SL curve is crossed. This form of extinction persists to $p(^T\mathrm{SL})$, but the amplitude of the periodic orbit at the onset of oscillation decreases as $p(\mathrm{H}_{10,1})$ is approached. Beyond $p(\mathrm{H}_{10,1})$ the amplitude grows in smoothly from zero. For a narrow range of pressures above $p(^T\mathrm{SL})$, the temperature interval on which oscillatory states appear is bracketed by intervals in which the reactor is in the ignited steady state. Extinction once again occurs upon reaching the left-hand branch of the SN curve. At first the oscillations grow in smoothly and disappear with large amplitude. At slightly higher pressures, a small, but discontinuous, increase in amplitude due to the presence of the $\mathrm{C}_1^{\mathrm{O}}$ point occurs at relatively high temperature (see Figure 6b), but the way in which the oscillatory state disappears is unaltered. A further slight increase causes the pressure to exceed $p(^T\mathrm{S}^{\mathrm{O}})$. This leads to the formation of an isolated branch of periodic orbits: the oscillations grow in from and return to zero amplitude over a temperature interval of steadily diminishing size and large amplitude oscillations are not observed if the temperature is simply ramped slowly downward (see Figure 6a). For pressures between $p(^T\mathrm{H}_{01})$ and $p(\mathrm{C}_1^{\mathrm{S}})$, classical extinction is observed.

Corroborating the Calculations: Some Suggested Experiments

The periodic-orbit isolas and intervals of birhythmicity are found at relatively high pressures. Dangers attendant to combustion reactions run at high pressure are an impediment to searching for these features, but our calculations minimize this impediment by providing guidance for conducting such a search systematically. In theory, a periodic-orbit isola like that shown in Figure 5 is impossible to detect by varying temperature alone. In practice, if a large step in temperature were taken on the branch of ignited steady states, it might perturb the reactor into the basin of attraction of the periodic orbit. However, not only is the likelihood of such a fortuitous perturbation small, but large changes in parameter are commonly avoided because they yield too coarse a resolution of the p-T diagram. Suppose instead that the reactor is in region IIIc and the pressure is raised while holding temperature constant. The reactor will arrive at an oscillatory state that is not isolated from the branch of steady states if p is the distinguished parameter but is isolated if T is the distinguished parameter. Restoring T as the distinguished parameter and identifying the endpoints of the interval of oscillatory dynamics as SNP bifurcations would verify the existence of the periodic-orbit isola.

Detecting birhythmicity of the type shown in Figure 6a depends on being able to find the isola. The high-temperature birhythmicity of Figure 6b would be detected by standard means, but the small temperature range might hinder the search. Distinct time series have been reported for reactor temperatures separated by as little as 1.5 K,[4] so even though the intervals of birhythmicity are only a few degrees in width, they should be detectable. Indeed, windows of birhythmicity as narrow in width as 2 K have been reported.[5] Locating the low-temperature birhythmicity of Figure 6b hinges on the accessibility of the stable ignited steady states to the left of the Hopf bifurcations. If ignition is to an oscillatory state and the reactor returns to the extinguished state upon reaching the low temperature limit of the branch of periodic orbits, these ignited steady states would be relatively difficult to find. If this were the case, a sequence of parameter changes similar to that used to reach the periodic-orbit isola offers a method for overcoming this difficulty. Once the reactor is on the low-temperature segment of the ignited steady-state branch, increasing the temperature leads to the small-amplitude periodic orbits beyond the low-temperature Hopf bifurcation.

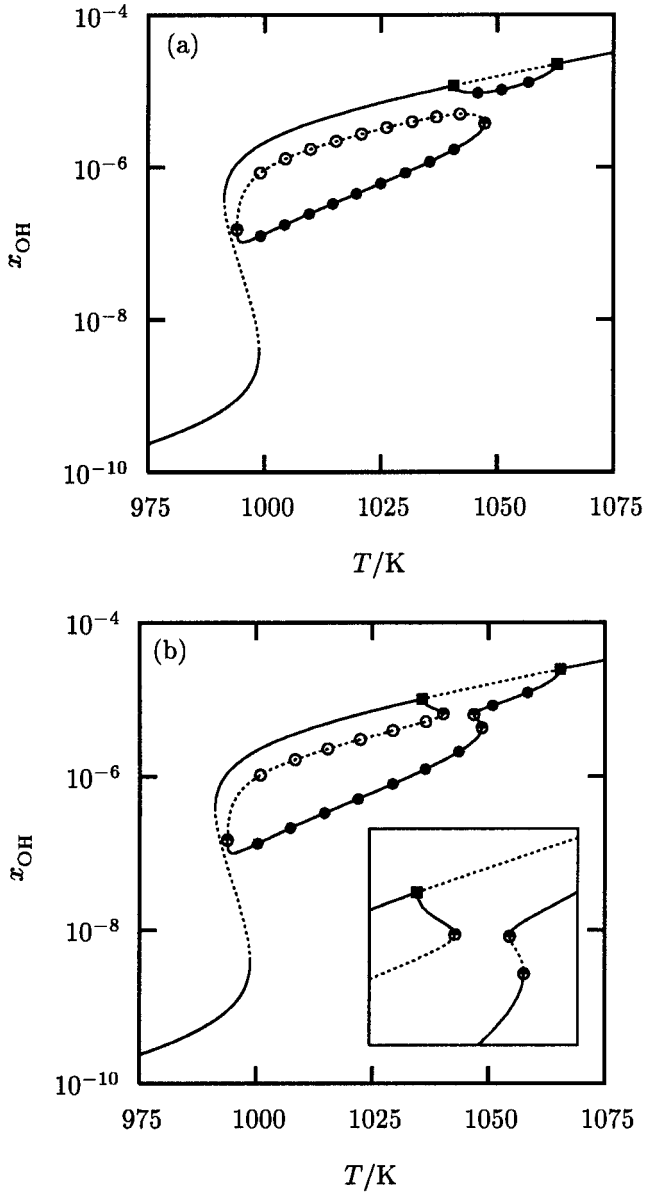

Figure 6. Bifurcation diagrams at 3.55 and 3.54 atm (3.597 and 3.587 bar). Hopf bifurcations are denoted by ■. At the higher pressure of (a) there is an interval of birhythmicity between the leftmost Hopf bifurcation and the rightmost SNP bifurcation (1040.7 to 1047.4 K). At the lower pressure of (b), there are two intervals of birhythmicity: one between the leftmost Hopf bifurcation and an SNP bifurcation (1035.7 to 1040.3 K) and the other between the two SNP bifurcations at the highest temperatures (1046.8 to 1048.5 K). The inset shows the orbit branch near the new SNP bifurcations on an expanded scale.

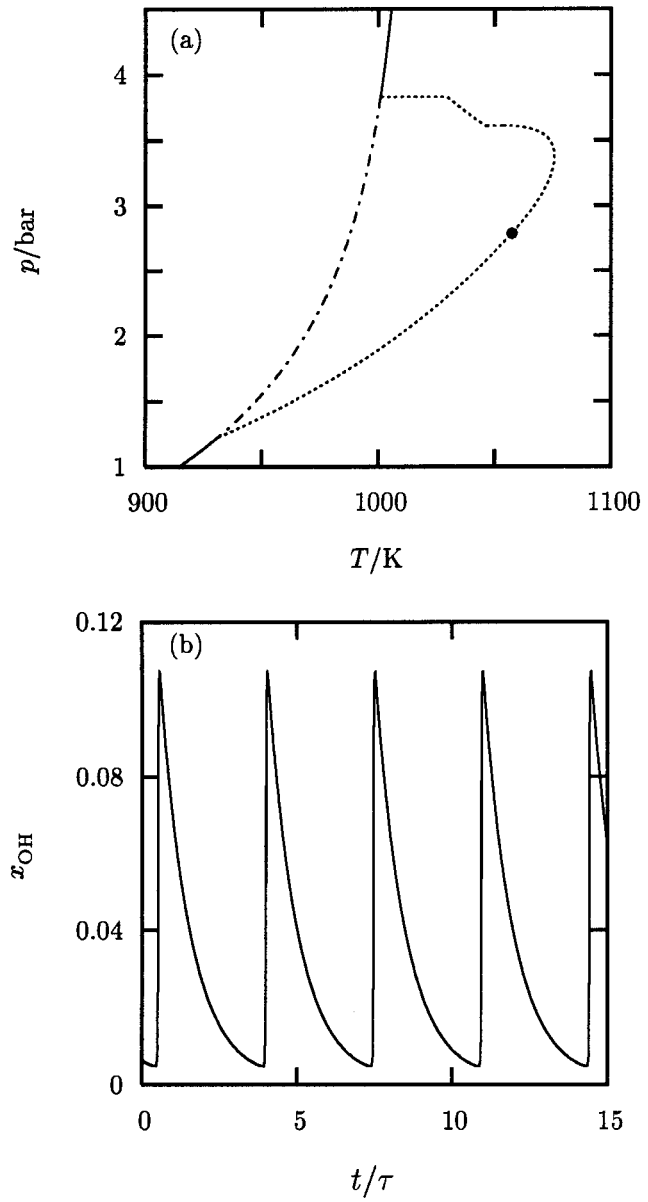

Figure 7. Predicted ignition dynamics. In (a) the transition from the extinguished state to steady ignition is indicated by —. Ignition to an oscillatory state (—•—) occurs at intermediate pressures. Transitions between oscillatory states and the ignited steady state are indicated by •••; oscillations disappear with nonzero amplitude except between ${}^{T}H_{01}$ (the fold with respect to temperature on the HB curve) and $H_{10,1}$. A representative oscillatory waveform ($p = 2.9$ bar) at the ignition point is shown in (b). The waveform is that of a relaxation oscillation, but the period is only about 3τ and x_{OH} remains significantly above zero at all times, thus confirming that this is not oscillatory ignition.

Even though millisecond residence times are technologically important, perfect mixing becomes increasingly difficult to attain as the residence time is shortened, and perfect mixing is implicit in our use of ordinary differential equations to model the reactor dynamics. Direct comparison of Figure 7a with extant experimental data is hindered because typical experiments are done at residence times about 1000 times longer than that of our simulations and because of the difficulty in maintaining isothermality. Bearing these points in mind, the most notable difference between an experimental *p*-*T* diagram such as Figure 2 of ref 4 and Figure 7a is the plateau on the curve marking the transition from oscillatory dynamics to steady ignition. Its presence reflects the existence of periodic-orbit isolas that are entirely outside the region of steady-state multiplicity. Following guideline G1, we have postulated that ignition to the isola takes place if the left-hand SNP bifurcation on the isola is within the region of steady-state multiplicity. If G1 is too strong an assumption, and ignition to an oscillatory state takes place only when the oscillatory state is the uniquely stable state, then the plateau of Figure 7a would be found at $p(\times_3)$. Preliminary calculations at residence times up to $\tau = 1$ s indicate that isola formation persists, so it would be worthwhile to undertake a systematic experimental search for such isolated branches of periodic orbits. In a series of experimental bifurcation diagrams, the plateau in Figure 8 would manifest itself as a discontinuity in the low-temperature limit of the oscillatory region and in the amplitude of the oscillatory state at its disappearance. At pressures above this plateau, the amplitude shrinks smoothly to zero as the temperature is decreased; below this segment,

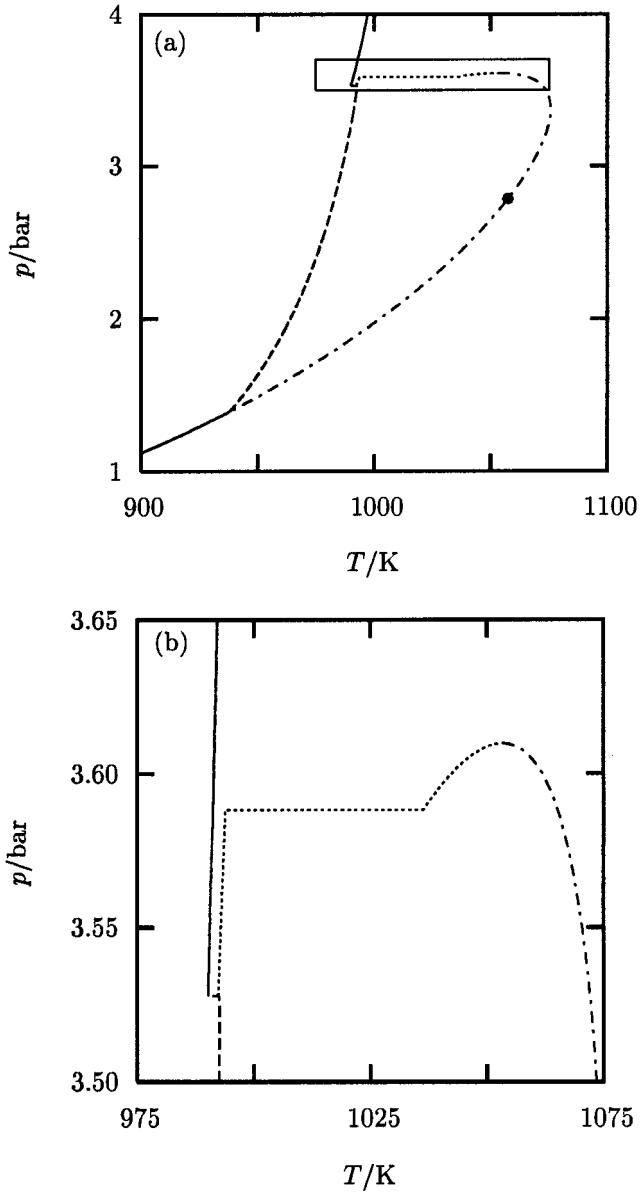

Figure 8. Predicted extinction dynamics. The onset of oscillations is demarcated by −•−. Oscillations appear with arbitrarily small amplitude above $H_{10,1}$. Disappearance of the oscillatory state leads either to a return to the ignited steady state (•••) or to extinction (- - -). (—) denotes both classical and premature extinction of the ignited steady state. The enclosed region of (a) is shown on an expanded scale in (b).

the oscillatory state has nonzero amplitude when it disappears.

Some cautionary notes related to our interpretation of the *p*-*T* diagram are in order. The appeal of phase portraits drawn as if the system were two-dimensional must not cause us to lose sight of the true, larger dimension of the set of rate equations. For sets of three or more equations, basins of attraction can be severely tangled. If two (or more) stable states remain upon disappearance of the state in which the reactor existed before the change in parameter, it is generally difficult to predict its asymptotic state. A second concern centers on the way in which the distinguished parameter is varied. Bifurcations can be delayed if the parameter is ramped up or down slowly.[24,25] On the other hand, large parameter changes can lead to an apparent crossing of basin boundaries; this is due to the accompanying large changes in the underlying structure of the trajectories and is distinct from the preceding concerns about tangled basins of attraction. Nevertheless, these complications do not preclude the interpretation we have developed, and it is well established that chemically reacting systems have small effective dimensions. We are not aware of any homogeneous-phase reactions of effective dimension greater than three (hyperchaos has been reported in the oxidation of CO on a Pt(110) surface).[26] To the best of our knowledge, a detailed explanation for the dramatic reduction in dimension in terms of the reaction kinetics has not been advanced; this connection may provide useful insights into combustion chemistry. Under the conditions of our simulations, we have found no evidence (e.g., chaotic states or steady states that are not "surrounded" by coexisting oscillatory states) requiring the $H_2 + O_2$ reaction in a CSTR at short residence times to be treated as having an effective dimension greater than two.

While these ambiguities of interpretation must be acknowledged, it should likewise be noted that they arise because of the attempt to compare experimental and calculated bifurcation diagrams, and experimental bifurcation diagrams are typically obtained by systematically increasing or decreasing a parameter such as temperature. This approach was entirely appropriate when calculated results were acquired solely by numerical integration, but, as we have shown here, it is now possible to compute a complete two-parameter description of the bifurcations associated with a large set of elementary reactions. In doing so, a great deal of new information becomes available. Although the experimental determination of ignition and extinction dynamics will continue to be important, additional emphasis can usefully be placed on determining phase portraits. If the calculated *p*-*T* diagram is complete, there is no ambiguity about the types and stabilities of the states that exist at a particular parameter value; comparison between experimental and calculated phase portraits over an extensive region of parameter space is a stringent test of the reaction set.

Conclusions

We have succeeded in obtaining a detailed, complete *p*-*T* diagram for a realistic set of elementary steps modeling the $H_2 + O_2$ reaction in an isothermal CSTR. Among the full collection of bifurcation diagrams in which temperature is the distinguished parameter, we find two types of birhythmicity and the first example of periodic-orbit isolas. The sequence of bifurcation diagrams containing periodic-orbit isolas accounts for nearly 15% of the pressure range over which stable oscillatory states exist. Both birhythmicity and isola formation occur at the high end of the pressure range, where the consequences of reactor runaway are most severe. Notwithstanding these dangers, practical processes are generally carried out at higher pressures. If work in the high-pressure regime is being contemplated, calculations such as ours provide valuable guidance for experimental design.

Confusing the lengthy quiescent intervals comprising almost all of a very-long-period orbit for an extinguished steady state could have grave consequences—the eventual burst of reactivity might cause catastrophic failure of the reactor. A mistake of this sort is possible because the burst of reactivity can occur hundreds of residence times after quasi-steady operation is erroneously identified as extinction. Such confusion is more likely for a periodic orbit near a saddle-node homoclinic bifurcation than for one near a saddle-loop homoclinic bifurcation because the lengthy quiescent interval bears a closer resemblance to the extinguished steady state in the former case. Moreover, the period of oscillation increases much more abruptly near a saddle-loop bifurcation, so the resemblance of the periodic orbit to a steady state exists over a much narrower parameter interval. Therefore, greater caution is required near

oscillatory ignition points and it is valuable to be able to distinguish between the two scenarios. Two-parameter curves of periodic orbits of very long period reliably approximate the two-parameter curves of infinite-period orbits needed for identification of oscillatory ignition. The saddle-loop and steady-state saddle-node curves are separated by about 5 K (the precise gap depends on the pressure). As a result, we predict that oscillatory ignition does not take place at short residence times ($\tau \approx 1$ ms) in a hydrogen−air mixture equimolar in hydrogen and oxygen. We plan to explore the position of the saddle-loop curve in relation to the steady-state saddle-node curve as residence time is increased and as the reactant mixture is changed from fuel-lean to fuel-rich.

Acknowledgment. We acknowledge partial support of this research by the donors of the Petroleum Research Fund, administered by the American Chemical Society, (R.J.O. & D.G.V.) and the Office of Naval Research with Dr. G. D. Roy through a Young Investigator Award under contract number N00014-96-1-0786 (D.G.V.). We thank Pierre Bui, Young Park, Preeti Aghalayam, Vladimiros Nikolakis, and Neil Fernandes for helpful comments and Simeen Sattar for a critical reading of an early version of the manuscript.

References and Notes

(1) Dixon-Lewis, G.; Williams, D. J. In *Gas-Phase Combustion*; Vol. 17 of *Comprehensive Chemical Kinetics;* Bamford, C. H., Tipper, C. F. H., Eds.; Elsevier: Amsterdam, 1977; Chapter 1.

(2) Lewis, B.; von Elbe, G. *Combustion, Flames, and Explosions of Gases*, 3rd ed.; Academic Press: Orlando, 1987.

(3) Gray, P.; Scott, S. K. *Chemical Oscillations and Instabilities: Nonlinear Chemical Kinetics*, Vol. 21 of *The International Series of Monographs on Chemistry*; Oxford University Press: Oxford, 1990.

(4) Johnson, B. R.; Griffiths, J. F.; Scott, S. K. *J. Chem. Soc., Faraday Trans.* **1991**, *87*, 523.

(5) Johnson, B. R.; Scott, S. K. *J. Chem. Soc., Faraday Trans.* **1997**, *93*, 2997.

(6) Chinnick, K.; Gibson, C.; Griffiths, J. F. *Proc. R. Soc. London, Ser. A* **1986**, *405*, 129.

(7) Guckenheimer, J.; Holmes, P. *Nonlinear Oscillations, Dynamical Systems, and Bifurcations of Vector Fields*, Vol. 42 of *Applied Mathematical Sciences;* Springer-Verlag: New York, 1983.

(8) Golubitsky, M.; Schaeffer, D. G. *Singularities and Groups in Bifurcation Theory: Vol. I*, Vol. 51 of *Applied Mathematical Sciences*; Springer-Verlag: New York, 1985.

(9) Guckenheimer, J. *Physica D* **1986**, *20*, 1.

(10) Vlachos, D. G. *Chem. Eng. Sci.* **1996**, *51*, 3979.

(11) Doedel, E. J.; Kernevez, J. P. AUTO: Software for Continuation and Bifurcation Problems in Ordinary Differential Equations (including the AUTO86 User Manual); Technical Report, Applied Mathematics, California Institute of Technology, 1986.

(12) Johnson, B. R.; Scott, S. K.; Tomlin, A. S. *J. Chem. Soc., Faraday Trans.* **1991**, *87*, 2539.

(13) Di Maio, F. P.; Barbieri, G.; Lignola, P. G. *J. Chem. Soc., Faraday Trans.* **1996**, *92*, 2989.

(14) Kalamatianos, S.; Vlachos, D. G. *Combust. Sci. Technol.* **1995**, *109*, 347.

(15) Kalamatianos, S.; Park, Y. K.; Vlachos, D. G. *Combust. Flame* **1998**, *112*, 45.

(16) Park, Y. K.; Vlachos, D. G. *J. Chem. Soc., Faraday Trans.* **1998**, *94*, 735.

(17) Olsen, R. J.; Epstein, I. R. *J. Chem. Phys.* **1991**, *94*, 3083.

(18) Olsen, R. J.; Epstein, I. R. *J. Chem. Phys.* **1993**, *98*, 2805.

(19) Glarborg, P.; Kee, R. J.; Grcar, J. F.; Miller, J. A. PSR: A Fortran Program for Modeling Well-Stirred Reactors; Technical Report SAND-86-8209, Sandia National Laboratories, 1986.

(20) Miller, J. A.; Bowman, C. T. *Prog. Energy Combust. Sci.* **1989**, *15*, 287.

(21) Miller, J. A.; Bowman, C. T. *Prog. Energy Combust. Sci.* **1990**, *16*, 347.

(22) Kee, R. J.; Rupley, F.; Miller, J. A. The CHEMKIN Thermodynamic Database; Technical Report SAND-87-8215B, Sandia National Laboratories, 1990.

(23) Kee, R. J.; Rupley, F.; Miller, J. A. CHEMKIN-II: A Fortran Chemical Kinetics Package for the Analysis of Gas-Phase Chemical Kinetics; Technical Report SAND-89-8009, Sandia National Laboratories, 1989.

(24) Erneux, T.; Laplante, J.-P. *J. Chem. Phys.* **1989**, *90*, 6129.

(25) Laplante, J.-P.; Erneux, T.; Georgiou, M. *J. Chem. Phys.* **1991**, *94*, 371.

(26) Eiswirth, M.; Kruel, T. M.; Ertl, G.; Schneider, F. W. *Chem. Phys. Lett.* **1992**, *193*, 305.

(27) Planeaux, J. B.; Jensen, K. F. *Chem. Eng. Sci.* **1986**, *41*, 1497.